Preprint
UCRL-JC-145879

Micromechanics of Transformation Superplasticity in Ti-6Al-4V/TiB_w Composites

C. Schuh, D. C. Dunand

This article was submitted to
2001 Fall Meeting of the American Society for Metals International Symposium on Superplasticity and Superplastic Forming, Indianapolis, IN., November 5-8, 2001

U.S. Department of Energy
Lawrence Livermore National Laboratory

October 16, 2001

DISCLAIMER

This work was performed under the auspices of the United States Department of Energy by the University of California, Lawrence Livermore National Laboratory under contract No. W-7405-Eng-48.

Micromechanics of Transformation Superplasticity in Ti-6Al-4V/TiB_w Composites

Christopher Schuh[1,2] and David C. Dunand[1]

[1] Department of Materials Science and Engineering, Northwestern University, Evanston, IL, USA, 60208
[2] Materials Science and Technology Division, Lawrence Livermore National Laboratory, Livermore, CA, USA, 94550

Abstract

Transformation superplasticity is a deformation mechanism induced by thermally-cycling a polymorphic material through the phase transformation range while simultaneously applying an external biasing stress. Unlike microstructural superplasticity, which requires a fine, equiaxed grain structure, this mechanism can be applied to coarse-grained alloys and composites. In this article, we review our research on transformation superplasticity of Ti-6Al-4V/TiB-whisker reinforced composites, during thermal cycling through the titanium α/β transformation range. The composites exhibit Newtonian flow and superplastic extension under these conditions. We describe the constitutive behavior of composites containing 0, 5 and 10 vol% reinforcing whiskers, and consider the effects of load transfer from matrix to whisker on superplastic deformation using existing rheological models. Additionally, strain hardening due to gradual whisker alignment is observed, and rationalized in terms of increased load transfer for aligned whiskers.

Introduction

The addition of reinforcing ceramic particulates to titanium or titanium alloys results in metal matrix composites with improved strength, stiffness and abrasion resistance [1, 2]. Titanium monoboride (TiB) is attractive because of its high hardness and stiffness, its low density and its chemical stability with titanium-based matrices [3]. Furthermore, during powder-metallurgy processing, TiB reinforcement can be synthesized *in situ* within the titanium alloy matrix by the dissolution of TiB_2 particles and subsequent re-precipitation of TiB, an orthorhombic phase with whisker morphology [3-6]. Similar microstructures can also be developed by rapid solidification processing of boron-containing titanium alloys [1, 2, 7, 8].

Since the addition of TiB reinforcement to titanium alloys reduces ductility and toughness [2, 9], traditional room-temperature forming techniques such as rolling, drawing, bending, stamping and machining are limited. High temperature processes such as forging are also much more difficult than for the unreinforced titanium alloy, while microstructural superplasticity, which relies on grain boundary sliding, can be ruled out for materials with matrix grains and reinforcements larger than about 10 μm.

Alternatively, polymorphic materials can be superplastically deformed by thermally cycling about their phase transformation range under the action of an externally-applied stress, independently of their grain size (for a recent review see Refs. [10, 11]). Internal transformation-mismatch stresses are biased by the external stress, and for uniaxial deformation the strain increment $\Delta\varepsilon$ produced on a complete thermal cycle is proportional to the applied stress σ. Repeated thermal cycling allows for the accumulation of superplastic strains (>100% in tension). Experimental studies of transformation superplasticity have demonstrated this effect for titanium [12-15], Ti-6Al-4V [16, 17], and composites of these materials containing equiaxed TiC particles in which the matrix transformation is used to drive deformation [13, 17, 18]. Some of our recent work has focused on transformation superplasticity of TiB whisker-reinforced titanium composites [19-21]. An additional issue with these composites is the alignment of the reinforcement in the matrix, which can lead to strength and stiffness enhancements in the direction of alignment.

In the present article, we summarize our investigations on tensile transformation superplasticity of Ti-6Al-4V reinforced with 5 or 10 vol. % TiB whiskers. We describe the constitutive linear relationship between superplastic strain increment and applied stress, and report tensile engineering strains in excess of 100%. Since the biasing stress on the matrix is affected by the whisker content and alignment, the deformation characteristics of these materials are modeled by considering issues of load transfer from matrix to reinforcement.

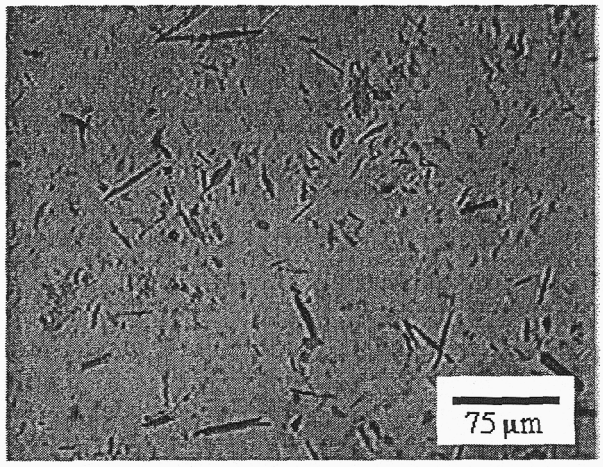

Figure 1: Unetched photomicrograph of as-received Ti-6Al-4V/10 vol% TiB material.

Materials and Methods

Specimens of Ti-6Al-4V reinforced with 5 or 10 vol. % TiB whiskers as well as unreinforced Ti-6Al-4V were supplied by Dynamet Technology (Burlington, MA), manufactured by their CHIP process [9, 22, 23], which consists of elemental powder blending, cold isostatic pressing, vacuum sintering, and containerless hot-isostatic pressing (HIPing). Titanium monoboride whiskers are produced *in-situ* by the addition of titanium diboride powders during the blending stage, which subsequently dissolve and re-precipitate as TiB whiskers during the sintering and HIPing stages [2, 4, 24].

A photomicrograph of the 10 vol% TiB-reinforced composite material in the as-received condition is shown in Fig. 1, with a fairly uniform distribution of randomly-oriented TiB whiskers with length of about 25-60 μm and aspect ratio of about 15-25. The homogeneity of the reinforcement distribution is reflective of the *in-situ* dissolution/reprecipitation which occurs during sintering, in which diffusion and allotropic transformation produced chemical and microstructural homogeneity on a fine scale. Etching exposed a matrix grain structure with an average grain diameter of 15-20 μm, smaller than in the unreinforced Ti-6Al-4V alloy, for which a matrix of large α grains (~150-250 μm diameter) and superimposed α-laths (~75-150 μm long) was observed. This type of microstructure is commonly observed upon slow cooling of Ti-6Al-4V from above the β-transus [25]. Because of the large and non-equiaxed microstructural dimensions of both of these materials, microstructural superplasticity by grain boundary sliding is not expected. Finally, both unreinforced Ti-6Al-4V and the Ti-6Al-4V/TiB composites were found to be fully dense (>99.8% theoretical for all materials) in the as-received condition.

The details of our tensile transformation superplasticity experiments and apparatus are available in Refs. [19, 20] and [26], respectively. The thermal cycles were symmetric triangles of 8-minute duration, between 840 and 1030° C, through the α/β transformation range of Ti-6Al-4V. This cycle profile was chosen to maximize the amount of transformation product (~75%), while providing ample time for the kinetics of the diffusional transformation. Two types of experiments have been performed. First, stress change experiments were used to determine the flow law during thermal cycling. The strain increment Δε after each thermal cycle was determined as a function of the applied uniaxial tensile stress, σ; reported values are averages over four or more consecutive thermal cycles. For these experiments the total engineering strain of the specimen was maintained below 15%, to avoid substantial reorientation of the TiB whiskers. Second, a single specimen of each material was deformed to fracture at an applied true stress of $\sigma = 2.5 \pm 0.1$ MPa, accounting for the cross-section reduction by assuming constant volume and uniform elongation.

The orientation of TiB whiskers with respect to the stress axis was investigated in the 10 vol%-reinforced materials, as reported in Ref. [19]. Texture data of both the matrix and reinforcing whiskers were obtained from Electron Back-Scatter Diffraction (EBSD) patterns obtained in a field emission scanning electron microscope at TexSEM, Inc. (Draper, UT). The accelerating voltage and specimen current were 20 kV and 1.0 nA, respectively, and about 20,000 patterns were acquired over an area of approximately 80,000 μm^2 for each sample analyzed. Between 148 and 495 individual TiB whiskers were identified on a given specimen.

Characteristics of Superplastic Flow

The superplastic strain increment Δε after each thermal cycle is shown in Fig. 2 as a function of the applied tensile stress for all of the experimental materials. For each, the relationship is linear, in agreement with the prevailing theory of transformation superplasticity by Greenwood and Johnson [12]:

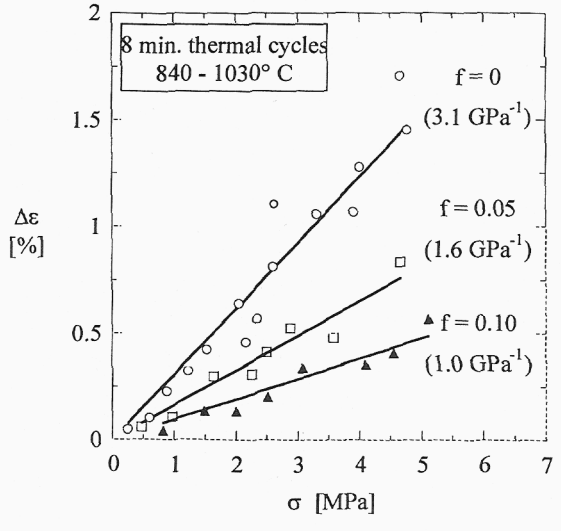

Figure 2: Strain increment Δε accumulated after each thermal cycle, as a function of the applied uniaxial tensile stress σ, for three whisker volume fractions, f.

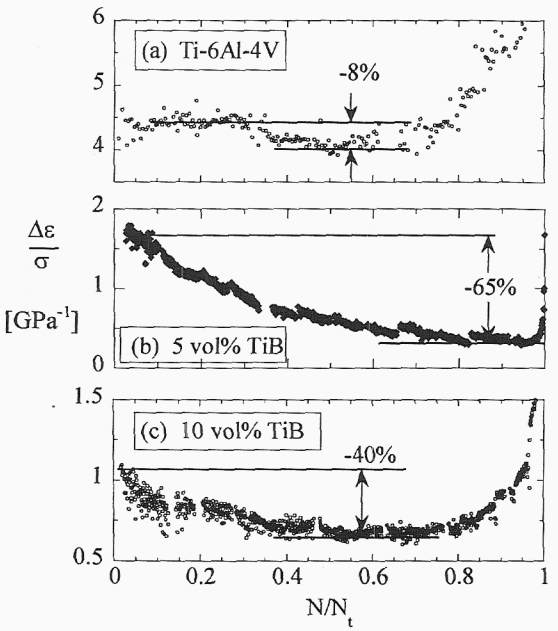

Figure 3: Stress-normalized strain increment ($\Delta\varepsilon/\sigma$) history of specimens deformed to failure: (a) unreinforced Ti-6Al-4V and (b) Ti-6Al-4V/5 vol %TiB or (c) Ti-6Al-4V/10 vol% TiB composites. N/N_t is the lifetime fraction of each specimen.

$$\Delta\varepsilon \approx \frac{4}{3}\cdot\frac{\Delta V}{V}\cdot\frac{5\cdot n}{4\cdot n+1}\cdot\frac{\sigma}{\sigma_o} \qquad (1)$$

in which $\Delta V/V$ is the volume mismatch between the polymorphic phases, n is the creep stress exponent of the phase which accommodates the mismatch strain, and σ_o is the time- and volume-averaged internal equivalent stress during the phase transformation. Although Eq. 1 was derived for an isothermal phase transformation (as for a pure allotropic metal), the linear result holds for alloys which transform over a range of temperatures, such as Ti-6Al-4V [27]. Furthermore, the internal strain due to thermal expansion-mismatch between matrix and TiB reinforcements is small compared to $\Delta V/V$. As illustrated by Fig. 2, The superplastic slope $d(\Delta\varepsilon)/d\sigma$ decreases monotonically with the volume fraction of reinforcement.

Fig. 3 shows the strain-increment history of the three specimens deformed to failure with σ = 2.5 MPa. Each strain increment is normalized by the instantaneous true applied stress to obtain the value of $\Delta\varepsilon/\sigma$ for each cycle, which is expected to be constant according to Eq. 1. For ease of comparison, the cycle number, N, is normalized by the total number of cycles to failure, N_t. Fig. 3a shows that the strain increment of Ti-6Al-4V was approximately constant for most of its deformation history, followed by a period of rapid increase associated with necking and/or cavitation prior to failure. From the beginning of the test until the onset of the final strain increment rise (similar to a creep tertiary stage), the maximum variation in the strain increment is about 8%. In contrast, the TiB-reinforced

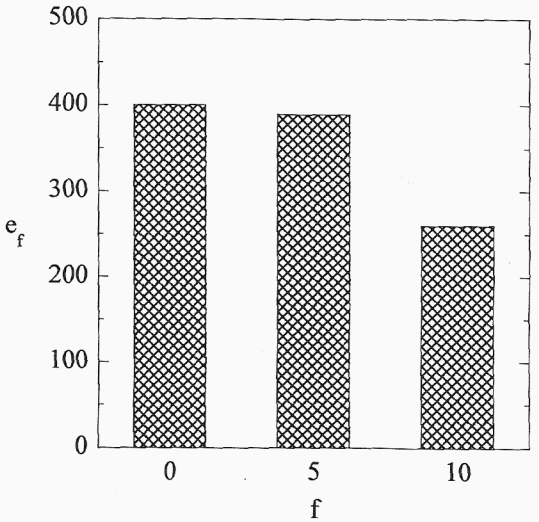

Figure 4: Effect of volume fraction f of reinforcing whiskers on elongation to failure (e_f) of Ti-6Al-4V/TiB composites, deformed during thermal cycling with applied stress σ = 2.5 MPa.

composites (Fig. 3b,c) experienced a significant reduction of the superplastic strain increment over the course of the experiment, by about 40-60% from the initial value. Because of this steady decrease, a true steady-state in the superplastic strain increment was not achieved.

As shown in Fig. 4, the addition of 5 vol% TiB only slightly reduces the achievable superplastic elongation of Ti-6Al-4V (from 398% to 390%). The addition of 10 vol% whiskers has a greater impact on the tensile ductility, reducing the elongation to failure by a factor of 1.5. Although the tensile ductility of these composites is substantial under thermal cycling conditions, the

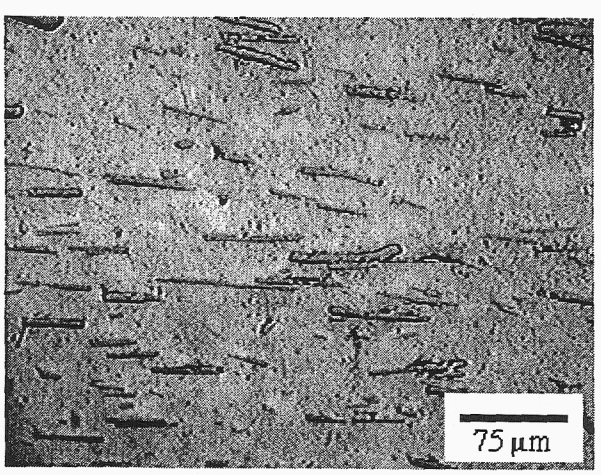

Figure 5: Optical micrograph of the 10 vol% TiB-reinforced composite deformed to failure with σ = 2.5 MPa. Tensile axis is horizontal.

whisker addition significantly reduces the deformation rate; the 5 vol% composite required about 800 thermal cycles (107 hours) to reach failure, compared with only 135 cycles (18 hours) for unreinforced Ti-6Al-4V to reach the same strain [19].

Microstructural Evolution

The optical micrograph in Fig. 5 shows a longitudinal section of the Ti-6Al-4V/10 vol% TiB composite deformed to failure at 260% engineering strain. Comparing with Fig. 1, the alignment of the TiB whiskers along the tensile axis (horizontal in Fig. 5) after deformation is noteworthy.

EBSD was used to identify the crystallographic orientation of the orthorhombic TiB phase in each of the four 10 vol% TiB specimens deformed to engineering strains of 0% (Fig. 1), 20.1%, 46.8%, and 260% (Fig. 5). Upon precipitation of TiB from the Ti-rich matrix during the sintering and HIPing stages of composite manufacture, growth of TiB occurs preferentially along the orthorhombic [010] direction [28, 29], resulting in the formation of whiskers with their longitudinal axes parallel to TiB-[010]. Thus, a standard texture analysis of TiB on a composite cross-section of known orientation allows for the identification of the whisker orientation with respect to macroscopic specimen dimensions.

We define the axial angle, ϕ, as the angle between the longitudinal dimension of the whisker (i.e., the TiB orthorhombic [010] direction) and the tensile axis. Then the angular orientation distribution, $P(\phi)$, is a probability density distribution subject to the normalization condition:

$$\int_0^{\pi/2} P(\phi)\cdot d\phi = 1 \qquad (2)$$

as well as two symmetry conditions:

$$P(\phi+\pi) = P(\phi) \qquad (3a)$$

$$P(-\phi) = P(\phi) \qquad (3b)$$

The probability of a randomly selected whisker exhibiting axial angle between ϕ and $\phi + \delta\phi$ is the integral of $P(\phi)$ with respect to ϕ over the given interval. From the EBSD results, the axial angle of each whisker was measured with an accuracy determined primarily by the sectioning procedure. We conservatively estimate this error as less than 5° based on visual observations after the sectioning procedure. Because EBSD determines texture on a surface, and not through the volume, a simple correction as described in Ref. [19] allows for calculation of the true distribution $P(\phi)$ representative of the entire specimen volume.

The distribution $P(\phi)$ determined from the experimental EBSD data for an as-received specimen as well as those deformed to engineering strains of 20.1%, 46.8%, and 260% (failure), corresponding to 0, 100, 200, and 625 thermal cycles, respectively. The tendency for whisker alignment with deformation is striking, with a pronounced TiB texture appearing after only 20.1% engineering strain. The expected

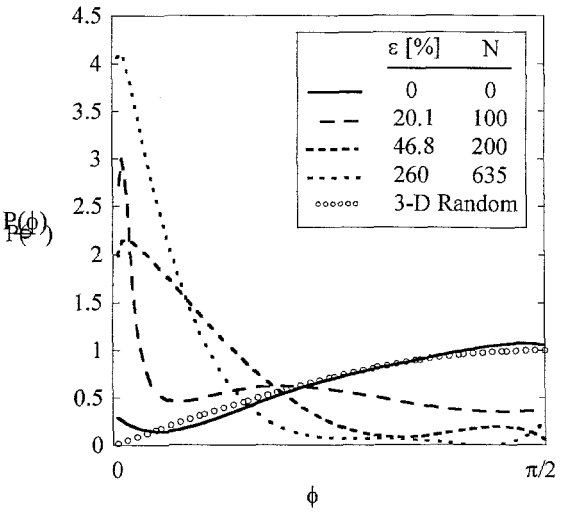

Figure 6: Probability density distributions for TiB whisker axial angles, ϕ, determined from electron backscattering diffraction data on 10 vol% TiB-reinforced composites. Distributions are shown for four specimens deformed to various engineering strains ε during N thermal cycles under 2.5 MPa applied tensile stress. The expected distribution for a 3-dimensionally random array of whiskers is also shown.

shape of $P(\phi)$ for a truly 3-dimensionally random distribution of whiskers is shown for comparison in Fig. 6. The good agreement between this distribution and that of the TiB in the as-received composite indicates that the powder metallurgy production route results in a nearly random distribution of whiskers. Local fluctuations in some of the distributions in Fig. 6 may be due to the small sampling size, and could perhaps be removed by sampling over a larger number of whiskers.

During uniaxial deformation, only the whisker axial angle ϕ is affected by the matrix flow, while the random distribution of azimuthal whisker angles is unchanged. EBSD data identifying the TiB-[100], and [111] directions indeed confirmed that the distribution of whisker azimuthal angles showed no texture before or after deformation. Therefore the microstructure remained transversely isotropic during all stages of the deformation. Finally, limited texture data of matrix α-grains was also acquired by the EBSD method, revealing no pronounced matrix texture either before or after deformation.

Load Transfer During Superplastic Deformation

Reinforcement volume fraction effect

The effect of TiB whisker reinforcement on transformation superplasticity of Ti-6Al-4V is summarized in Fig. 7, which shows the reduction in superplastic slope $(d(\Delta\varepsilon)/d\sigma$, equal to the inverse of viscosity for a Newtonian flow) as a function of the volume fraction of TiB, and normalized by the superplastic slope of the unreinforced matrix material, $d(\Delta\varepsilon)/d\sigma = 3.1\ GPa^{-1}$.

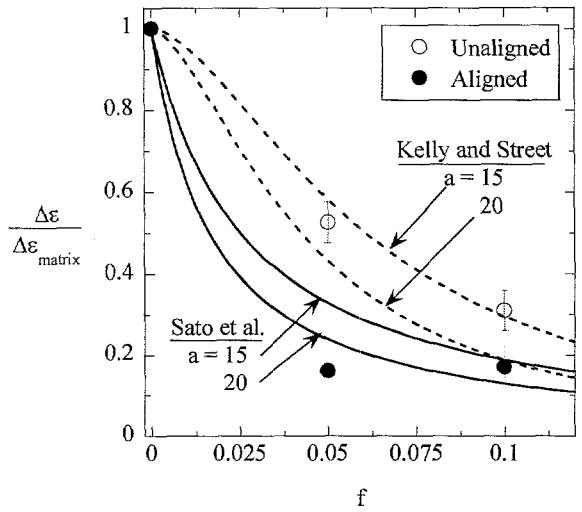

Figure 7: Reduction in the superplastic strain increment $\Delta\varepsilon/\Delta\varepsilon_{matrix}$ due to volume fraction f of reinforcing whiskers, at early stages of straining (i.e., with unaligned whiskers) and after superplastic straining (i.e., with strongly aligned whiskers). The analytical model predictions of Kelly and Street (11) and Sato et al. (12) (both for fully aligned whiskers) are also shown, for whisker aspect ratios a = 15 and 20.

The slope measured at early stages of straining (Fig. 2), when the whiskers are randomly-oriented, is shown, as well as the values obtained after superplastic elongation, when the whiskers are strongly aligned. Fig. 7 shows that the superplastic strain increments decrease with the reinforcement volume fraction, though this effect is more pronounced from 0 to 5 vol% than from 5 to 10 vol% TiB. In what follows, we consider the data in Fig. 7 in terms of existing models for creep of whisker-reinforced composites, which specifically consider the effect of load transfer.

Although the high-temperature creep of composites has been widely studied (see e.g., Refs. [30, 31] for an overview), there is no simple theoretical description for a power-law creeping matrix around large, rigid particles or whiskers. In the more simple case of a linear (Newtonian) matrix creeping around a rigid reinforcement, analytical solutions are possible, although they have little relevance to technologically important composites, which exhibit power-law creep behavior. Thus, transformation superplasticity represents a unique test case for the latter type of analytical model, because the matrix deforms on average according to a linear constitutive law, and the reinforcement particles can be reasonably assumed rigid.

One such model for creep of a whisker-reinforced metal is due to Kelly and Street [32]. These authors used a shear-lag mechanics approach, in which the whiskers are assumed aligned with the tension axis, and load transfer is assumed to occur only due to shear strain mismatch at the longitudinal matrix/whisker interfaces. For rigid fibers of aspect ratio a which are perfectly bonded to the matrix, these authors derived a closed-form solution for the steady-state creep rate of the composite, which, for the case of transformation superplasticity (i.e., Newtonian flow), reduces to:

$$\frac{\left(d(\Delta\varepsilon)/d\sigma\right)_{composite}}{\left(d(\Delta\varepsilon)/d\sigma\right)_{matrix}} = \frac{1}{1-f+f\cdot a^2\cdot S_1} \tag{4}$$

where the load transfer parameter S_1 is given by:

$$S_1 = \frac{2}{9}\cdot\left[\left(\frac{2\sqrt{3}}{\pi}\cdot f\right)^{-1/2} - 1\right]^{-1} \tag{5}$$

A second model for creep of a Newtonian matrix containing ellipsoidal particles is given by Sato et al. [33], who use the Eshelby equivalent inclusion method [34]. Assuming that ellipsoids are rigid and have their major axes aligned with the uniaxial applied stress, these authors derive the following expression, written here in terms of the superplastic slope:

$$\frac{\left(d(\Delta\varepsilon)/d\sigma\right)_{composite}}{\left(d(\Delta\varepsilon)/d\sigma\right)_{matrix}} = \frac{1-f}{1-f+f/S_2} \tag{6}$$

in which

$$S_2 = \frac{-9\cdot a^2}{2\cdot\left(a^2-1\right)^2} + \frac{3\cdot a\cdot\left(a^2+\frac{1}{2}\right)}{\left(a^2-1\right)^{5/2}}\cdot\operatorname{arccosh}(a) \tag{7}$$

In Fig. 7, the predictions of these two models (Eqs. 4 and 6) are shown as a function of the volume fraction of TiB, assuming an aspect ratio of a = 15 or 20. Both models predict significant decreases in the superplastic deformation rate with increasing TiB content. Moreover, both models predict a larger strengthening effect at lower volume fractions, and a gradual plateau at larger values of f, as exhibited by the experimental data.

Because both of the above models are formulated under the assumption of perfectly aligned whiskers, it is appropriate to compare their predictions with the solid points in Fig. 7, which represent superplastically deformed Ti-6Al-4V composite specimens with strongly aligned reinforcements. The model of Sato et al. [33] is very close to the experimental data after whisker alignment, while the shear-lag-based model of Kelly and Street [32] tends to under-predict the strengthening effect of the reinforcing whisker phase. However, Kelly and Street [32] have in fact noted that their model is expected to be most accurate for power-law creeping materials with stress exponents larger than unity.

Whisker alignment effect

During the course of superplastic deformation, the unreinforced Ti-6Al-4V alloy experienced only small relative variations in the strain increment $\Delta\varepsilon$ prior to the onset of failure (Fig 3a). Therefore, the considerable relative decrease in $\Delta\varepsilon/\sigma$ observed for the TiB-reinforced alloys (Fig. 3b,c) is likely an

effect stemming from the presence of the reinforcing phase, and not from other microstructural changes, such as grain growth. We propose that this decrease and lack of steady-state deformation of the composite is associated with the evolution of the whisker orientation distribution, P(ϕ), as shown in Fig. 6. This hypothesis is examined in more detail below.

In the present case, where the matrix is deforming plastically while the reinforcing phase is elastic, load transfer from matrix to reinforcement affects creep through the reduction of the matrix stress. For unreinforced metals and alloys, the uniaxial creep rate, $\dot{\varepsilon}_1$, is governed by the three average principal stresses σ_i (i = 1-3) according to a generalized creep equation [35]:

$$\dot{\varepsilon}_1 = A \cdot \sigma_{eq}^{n'-1} \cdot \left[\sigma_1 - \tfrac{1}{2}(\sigma_2 + \sigma_3)\right] \tag{8}$$

where A is a constant, σ_{eq} is the von Mises equivalent stress, and n' is the creep stress exponent. As the above generalized creep equation applies for many materials and deformation mechanisms, it can be adapted to transformation superplasticity by (i) replacing the average strain rate $\dot{\varepsilon}_1$ with the superplastic strain increment $\Delta\varepsilon_1$, and (ii) introducing the stress exponent n' = 1, since $\Delta\varepsilon$ is proportional to σ (Eq. 1). For axisymmetric microstructure and specimen geometry we take $\sigma_2 = \sigma_3$. Finally, upon the addition of an elastic reinforcing phase, we describe the plastic deformation as being governed by the average matrix stresses, σ_i^M. This assumption alone is inadequate to describe the deformation, as constraint of matrix flow by the reinforcement further reduces the deformation rate. Use of σ_i^M to describe the deformation thus requires the introduction of a geometric 'attenuation factor' which describes the fraction of the composite which flows under the average matrix stress. For our purposes, we take this factor to be independent of P(ϕ) and combine it with the existing constants in Eq. 1 to form a new constant, C. Then Eq. 8 becomes:

$$\Delta\varepsilon_1^C = C \cdot \left(\sigma_1^M - \sigma_2^M\right) \tag{9}$$

Predicting the effects of load transfer on deformation thus requires determining both the axial and transverse stresses in the matrix. We proceed by considering load transfer for a whisker inclined at axial angle ϕ, and extend to the case of a composite composed of many whiskers by summing the stress in each fiber given by the distribution P(ϕ). The whiskers are taken as load-bearing only along their major axis, and elastic load transfer is calculated using the shear-lag model [31, 36-38]. Throughout the following section superscripts of M and C will correspond to the matrix and composite, respectively.

We consider a unit cell as shown in Fig. 8, containing a single cylindrical whisker with axial angle ϕ with respect to the applied tensile stress. The coordinate system of the cell is differentiated from the global coordinate system with double-subscript notation, and the tensile axes for both systems are identical, $\sigma_1^C = \sigma_{11}^C$. In addition, a coordinate system aligned with the whisker axis is denoted by a prime.

In what follows, we describe a model developed in Ref. [19] to predict changes in elastic load transfer as a function of whisker alignment. During steady-state creep of discontinuously-reinforced composites, stress is partitioned between matrix and reinforcement according to the relative elastic moduli of the components (i.e., load transfer due to elastic strain-mismatch) as well as the creep behavior of the matrix (i.e., load transfer due to plastic strain-mismatch). The use of elastic calculations to estimate the stress partitioning between phases therefore neglects plastic strain mismatch, which includes two significant effects [31, 36-38]. First, plastic deformation of the matrix around an elastic particle increases strain mismatch between the phases, resulting in increased load transfer from matrix to whisker. Second, at high homologous temperatures, mismatch strains can be relaxed by stress-driven (i.e., mismatch-driven) diffusion or other relaxation processes. Neglecting the former effect results in overestimation of the stress borne by the matrix, while neglecting the latter effect has the opposite result. For a composite with large aspect-ratio reinforcement at high temperatures, diffusional relaxation can be expected to relieve some of the plastic strain mismatch–however, in general, both elastic and plastic strain mismatch still contribute to load transfer from matrix to reinforcement. The determination of the elastic contribution to load transfer therefore provides a lower-bound on the whisker stress, or an upper-bound on the matrix stress. For cases where relaxation processes are slow compared to the plastic deformation, more load is transferred to the whiskers, and elastic calculations quickly become inadequate. For the deformation of Ti-6Al-4V/TiB composites in the β-field of Ti-6Al-4V, the matrix self-diffusion is very rapid [39], so we anticipate significant

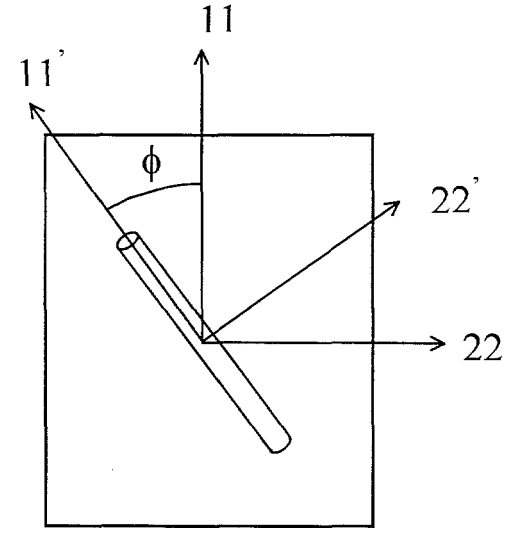

Figure 8: Geometry of the ideal unit cell considered in the elastic load transfer calculations, with principal coordinate systems for the cell (11- and 22-axes) and aligned with the whisker at axial angle ϕ (11'- and 22'-axes). The 33- and 33'- axes are coincident and normal to the page, and the global 1-axis is coincident with the local 11-axis.

relaxation of plastic strain mismatch and therefore a significant contribution to load transfer from elastic strain mismatch. Examination of superplastically deformed composites (Fig. (5)) shows no evidence of whisker fracture or of interfacial debonding, despite the extremely large plastic deformation of the matrix. This observation confirms that plastic strain-mismatch is substantially relaxed during transformation superplasticity.

Elastic load transfer from matrix to whisker with aspect ratio a is described by the shear-lag model, which gives the average axial stress in a single whisker, σ'^{W}_{11}, as a function of applied tensile strain along the whisker axis [31, 36-38]:

$$\sigma'^{W}_{11} = E^{W} \cdot \varepsilon'^{C}_{11} \cdot \chi \tag{10}$$

where E is Young's modulus, $\varepsilon'_{11}{}^{C}$ is the elastic strain of the unit cell in the 11'-direction, and the constant χ is given by:

$$\chi = 1 - \frac{\tanh(m \cdot a)}{m \cdot a} \tag{11}$$

with

$$m = \left[\frac{2 \cdot E^{M}}{E^{W} \cdot (1 + \nu^{M}) \cdot \ln(1/f)} \right]^{\frac{1}{2}} \tag{12}$$

and the Poisson's ratio ν.

For the assumption of elastic loading, we use Hooke's law to relate stress and strain, and apply tensor rotations to relate the coordinate system of the whisker with that of the unit cell. Details of derivation are available in Ref. [19], where the stress carried by a whisker at angle ϕ is derived as:

$$\sigma^{W}_{11} = E^{W} \cdot \chi \cdot \sigma^{C}_{11} \cdot \left(\frac{\cos^4 \phi}{E'^{C}_{11}} - \nu^{W} \cdot \frac{\sin^2(2\phi)}{4 \cdot E^{M}} \right) \tag{13a}$$

$$\sigma^{W}_{22} = E^{W} \cdot \chi \cdot \sigma^{C}_{11} \cdot \left(\frac{\sin^2(2\phi)}{4 \cdot E'^{C}_{11}} - \nu^{W} \cdot \frac{\sin^4 \phi}{E^{M}} \right) \tag{13b}$$

where

$$E'^{C}_{11} = (1 - f) \cdot E^{M} + f \cdot \chi \cdot E^{W} \tag{14}$$

The extension from the simple case of a single cell to a composite consisting of many adjacent unit cells requires a method of tessellation which provides realistic boundary conditions on each cell. This is a complex problem commonly encountered in finite-element modeling of discontinuously-reinforced composites [40]. In our case, differing whisker alignments in neighboring cells leads to aperiodic and unpredictable boundary conditions. However, in the dilute limit ($f \rightarrow 0$), each cell can be treated independently of its neighbors, i.e., each cell is subjected only to the externally-applied stress field. Furthermore, finite element calculations by Christman et al. [40] on elastic-plastic deformation of rigid aligned-whisker-containing composites have shown that the use of periodic or traction-free boundary conditions on such unit cells yields similar global deformation behavior in the elastic regime. We then proceed by assuming that the system is sufficiently dilute that the effects of boundary conditions between neighboring cells are small, and extend the simple case of a unit cell in tension to a composite consisting of many cells by the enforcement of mechanical equilibrium:

$$\left\langle \sigma^{M}_{1} \right\rangle = (1 - f)^{-1} \cdot \left\{ \sigma^{C}_{1} - f \cdot \left\langle \sigma^{W}_{11} \right\rangle \right\} \tag{15a}$$

$$\left\langle \sigma^{M}_{3} \right\rangle = \left\langle \sigma^{M}_{2} \right\rangle = -(1 - f)^{-1} \cdot f \cdot \left\langle \sigma^{W}_{22} \right\rangle \tag{15b}$$

where $\left\langle \sigma^{W}_{ii} \right\rangle$ is the average stress in all whiskers and $\left\langle \sigma^{M}_{i} \right\rangle$ is the average matrix stress. By means of Eqs. 15, the average stress in each whisker in the local coordinate system is related to the average stress carried by the matrix and the applied stress $\sigma_1{}^{C}$ in the global reference frame. Consistent with the condition of axisymmetry, Eq. 15b requires the equality of the two global transverse stresses.

Finally, the average stress in all whiskers is found by summing the stress of each individual whisker in the distribution $P(\phi)$:

$$\left\langle \sigma^{W}_{ii} \right\rangle = \int_{0}^{\pi/2} P(\phi) \cdot \sigma^{W}_{ii} \cdot d\phi \tag{16}$$

The average stress components in the matrix are now directly calculated by the use of Eqs. 13 and 16 in Eq. 15 and the introduction of appropriate materials parameters. Given these average matrix stresses, the deformation rate is given by Eq. 8, or, for transformation superplasticity of a transversely isotropic composite, by Eq. 9. Although we presently apply these calculations to the case of transformation superplasticity, they could also be applied more reasonably to cases of purely elastic loading, such as fiber fracture during low-temperature deformation [41], provided that the assumption of low volume fraction, as well as the many assumptions involved in the shear lag model, are valid.

In the following we apply the above equations to the case of

Table 1: Materials parameters employed in determination of the matrix/whisker load transfer for Ti-6Al-4V [25] and TiB [43] at ~900° C

	Ti-6Al-4V	TiB/TiB_2
E [GPa]	37	430
ν	0.32	0.14
a		20
f		0.1

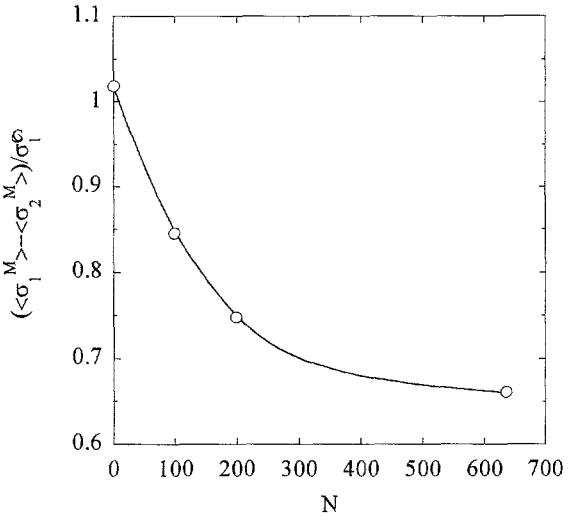

Figure 9: Deformation-controlling average stress term from Eq. 9 plotted vs. the number of thermal cycles for the Ti-6Al-4V/TiB composite. Each point corresponds to a successively larger degree of orientation of the reinforcing whiskers (Fig. 6).

superplasticity of Ti-6Al-4V/10 vol% TiB composites and determine the effect of the gradual whisker alignment on the superplastic strain increment. Eq. 16 is solved numerically using input parameters from Table 1, for the four whisker angle distributions in Fig. 6, allowing determination of the average matrix stresses at four points in the deformation history. Although we have experimentally determined the orientation distribution $P(\phi)$, predictions from existing models of whisker alignment during matrix flow (e.g. Ref. [42]) could alternatively be used as input to Eq. 15.

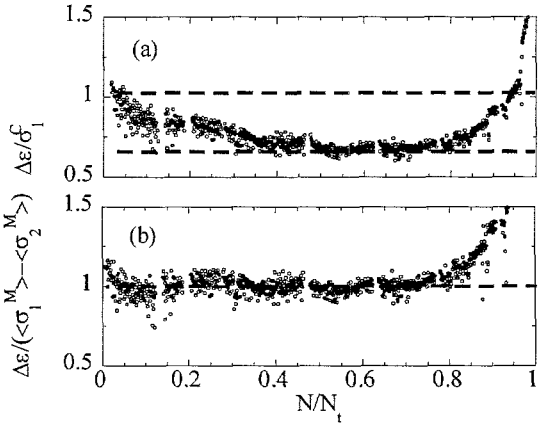

Figure 10: Strain increment history of Ti-6Al-4V/10 vol% TiB normalized (a) by the applied true stress, as in Fig. 4, and (b) by the deformation-controlling matrix stresses as per Eq. 9. N/N_t is the specimen life-time fraction.

The quantity $(<\sigma_1^M-\sigma_2^M>)/\sigma_1^C$, which governs the superplastic strain increment according to Eq. 9 is plotted as a function of N in Fig. 9, with the individual points corresponding to the whisker orientation distributions in Fig. 6. We note that the largest changes in matrix stress occur in the early stages of superplastic deformation, corresponding to the considerable whisker alignment observed after only 46.8% engineering strain (Fig. 6). One anomaly resulting from the present simple approach is the large matrix stress in the as-received case (N = 0), with random whisker distribution (Fig. 6), for which the majority of the whiskers lie at large angles to the loading axis. Since we assumed that the whiskers cannot bear load along their minor axes, and since shearing of the whiskers is neglected in the above analysis, the full load borne by such whiskers is underestimated and the matrix stress inflated. However, as the whiskers align and the average angle ϕ decreases, the calculations become more exact.

In Fig. 10b the strain increment $\Delta\varepsilon$ is shown normalized by the deformation-controlling matrix stress quantity, $(<\sigma_1^M>-<\sigma_2^M>)$, which has been interpolated between the four data points in Fig. 9. The original superplastic data for the 10 vol%-reinforced composite, normalized by the true applied stress (Fig. 3c), are replotted in Fig. 10a for ease of comparison. The two plots, Figs. 10a and 10b, then, respectively represent the strain increment history without and with load transfer effects considered. The result of normalization by the average matrix stresses, rather than the applied tensile stress, is two-fold. First, the large gradual decrease in strain increment observed in Fig. 10a is no longer present, replaced instead by a prolonged steady-state regime. Second, the onset of tertiary deformation behavior occurs earlier, now accounting for almost a third of the specimen lifetime. Indeed, these changes result in a strain increment history which closely resembles that of the unreinforced Ti-6Al-4V material (Fig. 3a). We conclude, therefore, that load transfer due to elastic strain mismatch between matrix and whiskers, and the gradual alignment of the whiskers, can explain the apparent strain-hardening observed during superplastic deformation for the Ti-6Al-4V/TiB composites. The lack of $\Delta\varepsilon$ dependence on N (for $N/N_t < 0.7$) in Fig. 10b may be somewhat fortuitous, considering the simplicity of the calculations and the many assumptions made.

Conclusions

We have investigated the effects of 5 or 10 vol% TiB whisker reinforcement on transformation superplasticity of Ti-6Al-4V, with the following notable results:

- By thermal cycling about the α/β phase transformation range of the matrix, we have measured superplastic tensile strain to failure of 390 and 260%, for composites containing 5 or 10 vol% reinforcing TiB, respectively. Additionally, the strain increment developed on each thermal cycle is proportional to the external tensile stress, giving an average strain-rate sensitivity of unity.
- We show that the deformation rate and achievable superplastic elongation decrease as the volume fraction of reinforcement increases. Additionally, we compare the experimental results to

two existing models for Newtonian creep around whisker reinforcements, and demonstrate that these results can be explained by load transfer from matrix to particle during deformation.

- Commensurate with gradual whisker alignment, a decrease in the superplastic strain rate and a lack of steady-state deformation behavior were observed. These effects can be justified by calculations which indicate that elastic strain-mismatch between matrix and whisker gradually increases during whisker alignment, leading to increased load transfer from matrix to whiskers.

Acknowledgements: This work was funded by the N.S.F. (SBIR grant #9901850 through a subcontract from Dynamet Technology, Burlington, MA), and CS was partially supported by the U.S. Department of Energy (through Lawrence Livermore National Laboratory, under grant W-7405-Eng-48).

References

1. S. Ranganath, *J. Mater. Sci.*, 32, 1-16 (1997).
2. R.J. Lederich, W.O. Soboyejo, and T.S. Srivatsan, *JOM*, 46, 68-71 (1994).
3. T. Saito, T. Furuta, and T. Yamaguchi, in *Recent Advances in Titanium Metal Matrix Composites*, F.H. Froes and J. Storer, eds., TMS, Warrendale, PA, 33-44 (1995).
4. K. Funami, M. Kobayashi, S. Suzuki, and C. Ouchi, *Mater. Sci. Forum*, 243-245, 515-20 (1997).
5. T. Saito, T. Furuta, and T. Yamaguchi, in *Metallurgy and Technology of Practical Titanium Alloys*, S. Fujishiro, D. Eylon, and T. Kishi, eds., TMS, Warrendale, PA, 351-62 (1994).
6. T. Saito, *Advanced Performance Materials*, 2, 121-44 (1995).
7. Z. Fan, P. Miodowinuk, L. Chandrasekaran, and M. Ward-Close, *J. Mater. Sci.*, 29, 1127-34 (1994).
8. S. Gorsse, J.P. Chaminade, and Y.L. Petitcorps, *Composites*, 29A, 1229-34 (1998).
9. S. Abkowitz, P.F. Weihrauch, and S.M. Abkowitz, *Industrial Heating*, 12, 32-7 (1993).
10. T.G. Nieh, J. Wadsworth, and O.D. Sherby, *Superplasticity in Metals and Ceramics*, Cambridge University Press, Cambridge (1997).
11. D.C. Dunand, in *International Conference on Thermomechanical Processing of Steels and Other Materials*, T. Chandra and T. Sakai, eds., TMS, Warrendale, PA, 1821-30 (1997).
12. G.W. Greenwood and R.H. Johnson, *Proc. Roy. Soc. Lond.*, 283A, 403-22 (1965).
13. D.C. Dunand and C.M. Bedell, *Acta Mater.*, 44, 1063-76 (1996).
14. Y. Takayama, N. Furushiro, and S. Hori, in *Titanium Science and Technology*, G. Lutjering, U. Zwicker, and W. Bunk, eds., Deutsche Gesellschaft fur Metallkunde,Munich, 753-60 (1985).
15. C. Chaix and A. Lasalmonie, *Res Mech.*, 2, 241-9 (1981).
16. K. Sato, T. Nishimura, and Y. Kimura, *Mater. Sci. Forum*, 170-172, 207-12 (1994).
17. C. Schuh, W. Zimmer, and D.C. Dunand, in *Creep Behavior of Advanced Materials for the 21st Century*, R.S. Mishra, A.K. Mukherjee, and K.L. Murty, eds., TMS, Warrendale PA, 61-70 (1999).
18. D.C. Dunand and S. Myojin, *Mater. Sci. Eng.*, 230A, 25-32 (1997).
19. C. Schuh and D.C. Dunand, *Int. J. Plastic.*, 17, 317-40 (2001).
20. C. Schuh and D.C. Dunand, *Scripta Mater.*, (2001).
21. M. Frary, C. Schuh, and D.C. Dunand, *Metall. Mater. Trans.*, in print, (2001).
22. S. Abkowitz and P. Weihrauch, *Adv. Mater. Proc.*, 136, 7, 31-4 (1989).
23. S. Abkowitz, P. Weihrauch, and S.M. Abkowitz, in *Titanium Science and Technology '92*, F.H. Froes and I. Caplan, eds., Warrendale PA: TMS, 2511-9 (1993).
24. T. Yamamoto, A. Otsuki, K. Ishihara, and P.H. Shingu, *Mater. Sci. Eng.*, A239-240, 647-51 (1997).
25. *Metals Handbook: Properties and Selection: Nonferrous Alloys and Pure Metals*, American Society for Metals, Metals Park, OH (1979).
26. P. Zwigl and D.C. Dunand, *Metall. Mater. Trans.*, 29A, 2571-81 (1998).
27. C. Schuh and D.C. Dunand, *Acta Mater.*, 49, 199-210 (2001).
28. D.X. Li, D.H. Ping, Y.X. Lu, and H.Q. Ye, *Mater. Let.*, 16, 322-6 (1993).
29. M.E. Hyman, C. McCullough, J.J. Valencia, C.G. Levi, and R. Mehrabian, *Metall. Trans.*, 20A, 1847-59 (1989).
30. D.C. Dunand and B. Derby, *Creep and Thermal Cycling*, in *Fundamentals of Metal Matrix Composites*, S. Suresh, A. Mortensen, and A. Needleman, Editors. 1993, Butterworth-Heinemann: Boston. p. 191-214.
31. T.W. Clyne and P.J. Withers, *An Introduction to Metal Matrix Composites*, Cambridge University Press, Cambridge (1993).
32. A. Kelly and K.N. Street, *Proc. Roy. Soc. Lond.*, A328, 283-93 (1972).
33. E. Sato, T. Ookawara, K. Kuribayashi, and S. Kodama, *Acta Mater.*, 46, 4153-9 (1998).
34. J.D. Eshelby, *Proc. Roy. Soc. Lond.*, A241, 376-96 (1957).
35. I. Finnie and W.R. Heller, *Creep of Engineering Materials*, McGraw-Hill, New York (1959).
36. H.L. Cox, *Brit. J. Appl. Phys.*, 3, 72-9 (1952).
37. V.C. Nardone and K.M. Prewo, *Scripta Metall.*, 20, 43-8 (1986).
38. T.W. Clyne, *Mater. Sci. Eng.*, A122, 183-92 (1989).
39. H.J. Frost and M.F. Ashby, *Deformation-Mechanism Maps: The Plasticity and Creep of Metals and Ceramics*, Pergamon Press, Oxford (1982).
40. T. Christman, A. Needleman, S. Nutt, and S. Suresh, *Mater. Sci. Eng.*, A107, 49-61 (1989).
41. Y.L. Klipfel, M.Y. He, R.M. McMeeking, A.G. Evans, and R. Mehrabian, *Acta Metall. Mater.*, 38, 1063-74 (1990).
42. F. Folgar and C.E. Tucker.III, *J. Reinforced Plastics and Composites*, 3, 98-119 (1984).
43. *Engineered Materials Handbook, Vol 4. Ceramics and Glasses*, ASM International, Metals Park, OH (1987).